Dual fiber optical trapping in a polymer-based microfluidic chip

Ottevaere, Heidi; De Coster, Diane; Vervaeke, Michael; Van Erps, Jürgen Albert; Callewaert, Manly; Wuytens, Pieter; De Malsche, Wim; Thienpont, Hugo

Published in:
Micro-Optics 2016

DOI:
10.1117/12.2227917

Publication date:
2016

Document Version:
Final published version

Dual fiber optical trapping in a polymer-based microfluidic chip

Heidi Ottevaere[1], Diane De Coster[1], Michael Vervaeke[1], Jürgen Van Erps[1], Manly Callewaert[1,2], Pieter Wuytens[1], Wim De Malsche[2] and Hugo Thienpont[1]
[1]Vrije Universiteit Brussel, Dept. Of Applied Physics and Photonics, Brussels Photonics Team, Pleinlaan 2, 1050 Brussel, Belgium
[2]Vrije Universiteit Brussel, Dept. of Chemical Engineering (CHIS), Pleinlaan 2, 1050 Brussel, Belgium

ABSTRACT

We present a microfluidic chip in Polymethyl methacrylate (PMMA) for optical trapping of particles in an 80µm wide microchannel using two counterpropagating single-mode beams. The trapping fibers are separated from the sample fluid by 70µm thick polymer walls. We calculate the optical forces that act on particles flowing in the microchannel using wave optics in combination with non-sequential ray-tracing and further mathematical processing. We use a novel fabrication process that consists of a premilling step and ultraprecision diamond tooling for the manufacturing of the molds and double-sided hot embossing for replication, resulting in a robust microfluidic chip for optical trapping. In a proof-of-concept demonstration, we show the trapping capabilities of the hot embossed chip by trapping spherical beads with a diameter of 6µm, 8µm and 10µm and use the power spectrum analysis of the trapped particle displacements to characterize the trap strength.

Keywords: trapping, polymers, diamond machining, microstructure fabrication, micro-optical devices

1. INTRODUCTION

Cell identification is important to differentiate between cells in a sample. In cancer research for example, there is a need for identifying tumor cells and discriminating these from healthy cells. Raman spectroscopy is a non-destructive label-free method that can be used for the analysis of biological or chemical samples by determining the molecular fingerprint of molecules or cells [1-2]. Since Raman scattering is a weak process, the molecular fingerprint of flowing particles would be hard to measure. The low efficiency of Raman scattering can be enhanced using special surface structures, i.e. surface-enhanced Raman spectroscopy (SERS) [3] but these specialty surfaces are difficult to mass-produce. An alternative method is to stably position the cell under test in the detection area during acquisition of the Raman scattering such that the acquisition time can be increased. Positioning of cells can be done through optical trapping and leads to an enhanced signal-to-noise ratio and thus a more reliable cell identification. The work of Ashkin in 1970 demonstrated the capability of using two counterpropagating laser beams to optically trap a particle [4]. Optical trapping is a non-contact optical manipulation technique that can trap, move and sort cells using optical forces [5] and has led to a lot of biological and biomedical applications [6].

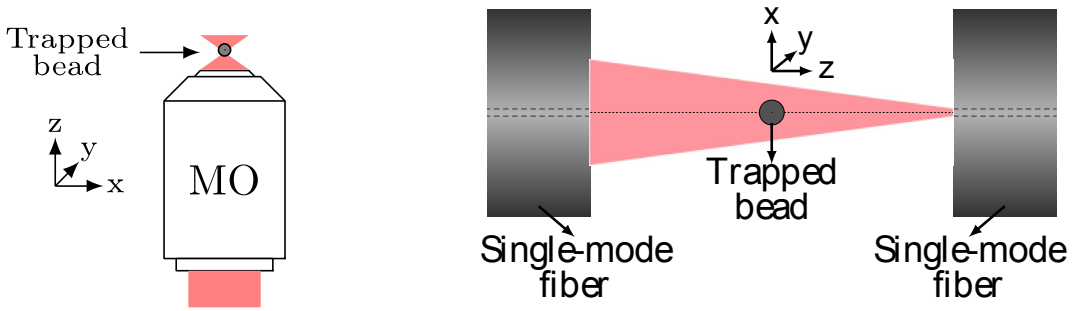

Figure 1: (a) An optical tweezer traps particles based on a single beam focused by a high numerical aperture microscope objective (MO); (b) A dual fiber optical trap traps particles based on two counter-propagating divergent single-mode beams.

Micro-Optics 2016, edited by Hugo Thienpont, Jürgen Mohr, Hans Zappe, Hirochika Nakajima, Proc. of SPIE Vol. 9888, 98880B · © 2016 SPIE
CCC code: 0277-786X/16/$18 · doi: 10.1117/12.2227917

The interaction of light with matter gives rise to optical forces, which can optically confine a particle in a light beam under certain conditions. The optical forces exerted by a light beam on a particle are often divided in gradient forces (transverse to the light propagation, in the direction of the intensity gradient of a Gaussian beam) and scattering forces (in the direction of the light propagation). Both forces have the same physical origin, this separation is merely a way to conveniently discuss the optical force. A Gaussian beam (TEM00) is the most commonly used beam profile in optical tweezers, which is an optical trap based on a single beam focused by a high numerical aperture microscope objective (MO), also called a single beam gradient trap (Fig. 3.1(a)). A Gaussian beam can be focused to the smallest diameter beam waist and will therefore produce an efficient and harmonic trap [7]. Also in a dual fiber optical trap configuration, based on two counterpropagating divergent single-mode beams, Gaussian beams are commonly used to have one stable trapping position (Fig. 3.1(b)). The advantages of a single beam gradient trap is that strong traps can be achieved (trapping efficiency $Q \approx 0.25\text{-}0.35$ for 10μm diameter polystyrene beads [8]). A disadvantage is that the particle will be trapped in the region with the highest refractive index, which is the nucleus in case of cells. Another disadvantage is the risk of cell photo-damage when using a highly focused beam. The advantages of a dual fiber optical trap is that using two opposing divergent beams reduces the risk of photo-damage and that the large confinement region of this kind of optical trap leads to its capability to stably hold and manoeuver large cells. The main disadvantage of this dual fiber optical trap is that trapping forces are lower (trapping efficiency $Q \approx 0.07$ for 10μm diameter polystyrene beads, 220μm trapping fiber separation) compared to the forces achieved in a single beam gradient trap. Because of its compatibility with a microfluidic device we choose to work on dual fiber optical traps.

In this paper we introduce a design and fabrication method for integrated particle manipulation in which fiber-optic laser beams are used to optically trap particles in a microchannel. The novelty of this device lies in the mass-manufacturing which allows a low-cost microfluidic chip. The chip is made of PMMA and is robust, which is obtained due to the design of the chip and the use of double-sided hot embossing. We first introduce the model used for calculating the trapping forces and validate it theoretically and experimentally. Next, we discuss the prototyping process of the PMMA chip consisting of a premilling step and ultra-precision diamond tooling for the mold fabrication and subsequent replication through hot embossing. We characterize the fabricated microstructure and discuss the sealing method of a PMMA top layer to make the microchannel leakproof, resulting in an assembled chip for optical trapping. Finally, we use the chip in a proof-of-concept demonstration setup to trap polystyrene microbeads with a diameter of 6μm, 8μm and 10μm and discuss the detection method and the resulting forces.

2. Modelling and design of mass-manufacturable polymer microfluidic device for dual fiber optical trapping

2.1. Introduction of model using wave-optics and non-sequential ray-tracing

In this work we will use a wave-optics and ray-tracing model in a non-sequential ray-tracing environment to calculate optical forces acting on particles in an optical trap. The model can calculate the force and torque on spherical and non-spherical (e.g. cylindrical) particles, for different positions and orientations of a particle in the laser beam. With the knowledge of both the optical forces and the optical torque acting on a particle, we can in principle predict the entire trajectory of a particle in a light beam. Also other types of beam profiles could be simulated by the 'Gaussian Beam Propagation' method we adopted in our model. With this method, we achieve an accurate propagation of a Gaussian trapping beam in and outside the Rayleigh range. In order to verify our model we compared the optical force in a dual fiber optical trap immersed in water with the analytical solution presented in literature [9], for a spherical particle. This comparison showed a good agreement between the simulated and numerically integrated trapping force, but both calculations were based on a ray-tracing approach. To our knowledge, the model developed in [10] for the calculation of optical forces acting on a particle in an optical trap, has more functionalities than those proposed in literature. The calculation of optical torque was demonstrated by Aspnes et al. [11]. However, their model was not able to propagate a Gaussian beam near the Rayleigh range. They also used sequential ray-tracing, which makes it impossible to consider interaction of back-reflected rays. Furthermore, they only considered optical forces acting on spherical particles. A method for the realistic propagation of Gaussian beams close to the Rayleigh range is also found in the work of Ferrera et al. [12], but their model can only cope with spherical particles and does not allow the calculation of optical torque. Furthermore, they can only calculate optical forces exerted by a circular Gaussian beam, while we are able to propagate an arbitrary wavefront, as long as the paraxial wave approximation is valid. Sray et al. [13] developed a dynamic ray-tracing model that calculates the deformation of an elastic surface due to optical forces, which in turn changes the optical

forces acting on the particle. Their model did not allow propagation of a Gaussian beam and could not calculate optical torque. Furthermore, it did not allow to consider the interaction of back-reflected rays. The benefits of our model are that the non-sequential ray-tracing allows to take into account the interactions of back-reflected rays and that the 'Gaussian Beam Propagation' method allows a realistic propagation of Gaussian beams in and near the Rayleigh range.
The dielectric particle to be trapped can also have a non-spherical shape, for which we can calculate both the optical force and torque exerted on this particle. In the remainder of this work we consider uniform spherical particles. A more realistic modelling of biological particles could be achieved by representing them as a particle containing different dielectric zones with a different refractive index.

2.2. Introduction of the novel on-chip optical trapping design

In this design, we use a microchannel with a width of 80µm and a height of 320µm. The channel is separated from the trapping fibers by walls with a thickness of 70µm, preventing contamination of the trapping fibers by the sample fluid flowing in the microchannel, which leads to a total fiber separation of 220µm. These dimensions were chosen as a compromise between the chip robustness and the optical trapping strength. A schematic drawing of the design is shown in Figure 2. In the axial direction the trap is formed by balancing the radiation pressure applied by either beam. If the particle is displaced in the positive z direction, then the radiation pressure from the beam travelling in the negative z direction increases, providing a restoring force. This differs from other counterpropagating beam traps, in which the focal point of the beams are superimposed and axial trapping is achieved by the gradient forces [14]. In the transverse direction, the optical trap relies on gradient forces originating from the intensity profile of the single mode Gaussian beams. To qualitatively evaluate the optical forces that act on particles flowing in the trapping area in the microchannel between the two counterpropagating laser beams, we use the wave optics and ray-tracing model combined with mathematical processing, introduced in the previous section.

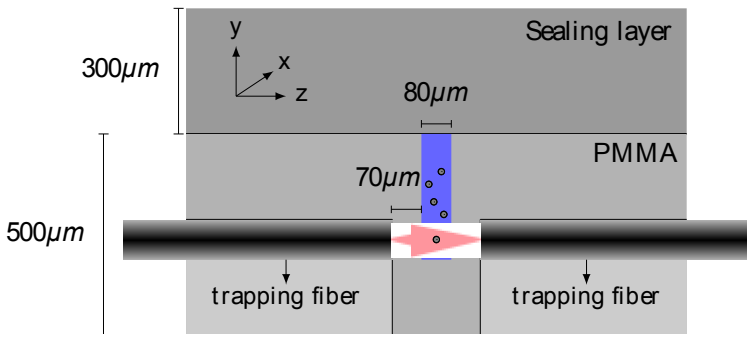

Figure 2: Schematic cross-section of the microchannel in the chip at the position of the fibers. A particle is trapped in the center of the channel by two divergent light beams emitted by the trapping fibers. The channel is sealed at the top by a second PMMA layer [10].

In this work we use a TEC-510-0785-300 Littman/Metcalf laser from Sacher Lasertechnik, emitting a laser beam with a fixed wavelength of 785nm. The laser light is coupled into a single mode pigtail (PM780-HP fiber) through a single-mode fiber coupler at the laser exit. This fiber has a mode field diameter (MFD) of 5µm at 785nm, a numerical aperture (NA) of 0.12 and a cutoff wavelength of 710±60nm, which is the wavelength at which the V-number is approximately equal to 2.405 and the wavelength above which only the fundamental mode propagates. Higher order modes will start propagating below this cutoff wavelength and the fiber will become multimode. Since our trapping wavelength is 785nm and higher than the cutoff wavelength, this fiber will only carry the fundamental mode. The splitter should also be compatible with the PM780-HP pigtail. The coupling of the pigtailed laser to the fiber splitter introduces an insertion loss (typically 0.15dB). At each output of the splitter we need to connect a trapping fiber with an open end at its other extremity to deliver the laser light to the trap. This will again give rise to an insertion loss (typically 0.15dB). The trapping fibers are single-mode fibers with a mode field diameter of 5µm±0.5µm (core diameter = 4.4µm) at 850nm and a numerical aperture of 0.13. The cut-off wavelength is 730±30nm. With the information about the core, the numerical aperture and the trapping wavelength we calculate the V-number of the trapping fibers which is equal to 2.2892. Using

the 785nm wavelength and these parameters for the trapping fibers, we can do an in-depth theoretical validation of the trapping efficiencies.

We apply our model to the dual fiber optical trap configuration with the trapping fibers directly inserted in water and compare it first with an existing analytical solution based on the formula used by Sidick et al. [15] (Eq. 1) which gives the trapping efficiency in the ray-tracing regime for a spherical bead in a Gaussian beam.

$$\vec{Q} = \frac{4r_0^2}{\pi}\int_0^{2\pi} d\phi \int_0^{\theta_{max}} d\theta \sin(\theta) \times \cos(\theta)(\vec{s}q_s + \vec{g}q_g)\frac{\exp(-2r^2/w^2)}{w^2} \tag{1}$$

We also recall the formula relating the trapping efficiency and force [15]:

$$\vec{Q} = \frac{c}{n_l \cdot P}\vec{F} \tag{2}$$

with c the speed of light in vacuum, n_l the refractive index of the medium, P the total power and F the optical force. The transverse trapping efficiency is calculated with our model and by numerical calculations, in the case of a dual fiber optical trap immersed in water with a fiber separation distance of 160µm. We choose to do the validation of our model using this 160µm separation distance instead of the 220µm indicated in Figure 2 to limit the number of basis functions in the Mie theory calculation. Also experiments with a 160µm separation distance (using a square microcapillary) will be done. We work with a wavelength of 785nm, a beam waist of 2.5µm and consider polystyrene (npolystyrene = 1.579 at 785nm [16]) spherical beads in water (n_{water} = 1.33 at 785nm [16]) with a radius of 3µm, 4µm, 5µm and 7.5µm. We observe a good agreement (maximal deviation 8%) between the analytical model and our ray-tracing approach. Due to the centrosymmetric profile of the Gaussian beams and the spherical symmetry of the bead, the trapping behavior is the same in the other transverse direction (y).

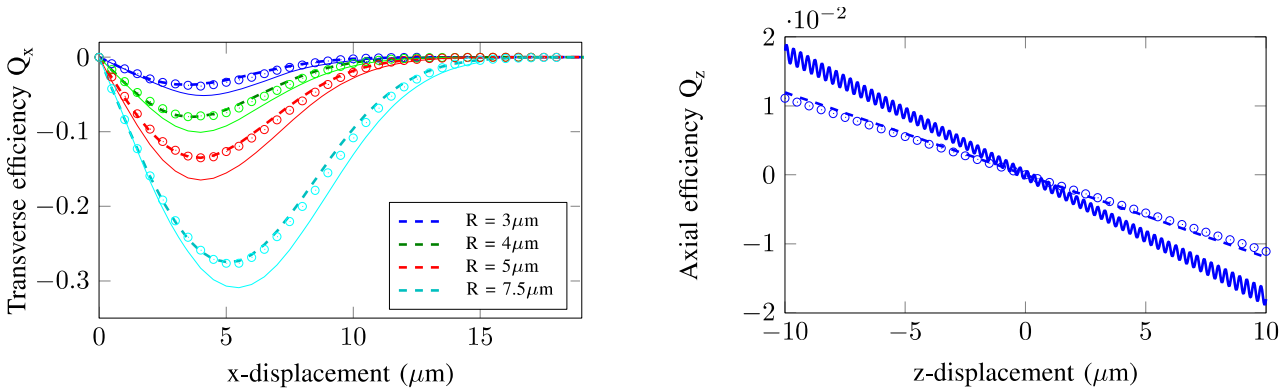

Figure 3: (a) Transverse trapping efficiency as a function of the x-displacement from the equilibrium position for beads with a radius of 3µm, 4µm 5µm and 7.5µm for a fiber separation of 160µm, calculated with our ray-tracing model (circles), the analytical solution (dashed line) and the T-matrix method (solid line); (b) Axial trapping efficiency as a function of the z-displacement from the equilibrium position for a bead with a radius of 3µm and for a fiber separation of 160µm, calculated with our ray-tracing model (circles), the analytical solution (dashed line) and the T-matrix method (solid line).

3. Fabrication of the hot embossed optical trapping chip

The fabrication process of the optical trapping chip consists of different steps. First, two molds are manufactured through premilling and ultraprecision diamond tooling (Moore, Nanotech 350FG). These two mold are needed to realize a component as schematically drawn in Figure 4a, consisting of an overlapping area between the microchannel and the fibergrooves within the chip, where the trapping of the particles under test will take place. One mold (i.e. 'Channel mold') contains the inversed microchannel and the other mold (i.e. 'Fiber mold') the inversed fiber grooves. In a next step, these molds are used in a double-sided hot embossing process (Jenoptik, HEX04), which results in a microstructured PMMA layer containing a 80µm wide microchannel and two grooves for the single-mode fiber

alignment (see Figure 5). Finally, a PMMA toplayer is bonded to the hot embossed layer to seal the microchannel and microcapillaries are introduced at both ends of the channel to allow particles to flow in the microchannel. Before starting up the fabrication run, the channel and the fiber molds were designed using 'Spaceclaim' computer-aided design (CAD) software. This is necessary to verify if these molds lead to the targeted microstructured PMMA layer and that no contact between the molds will occur when an overlap is achieved between the channel- and fiber microstructure within the chip (see Figure 4b).

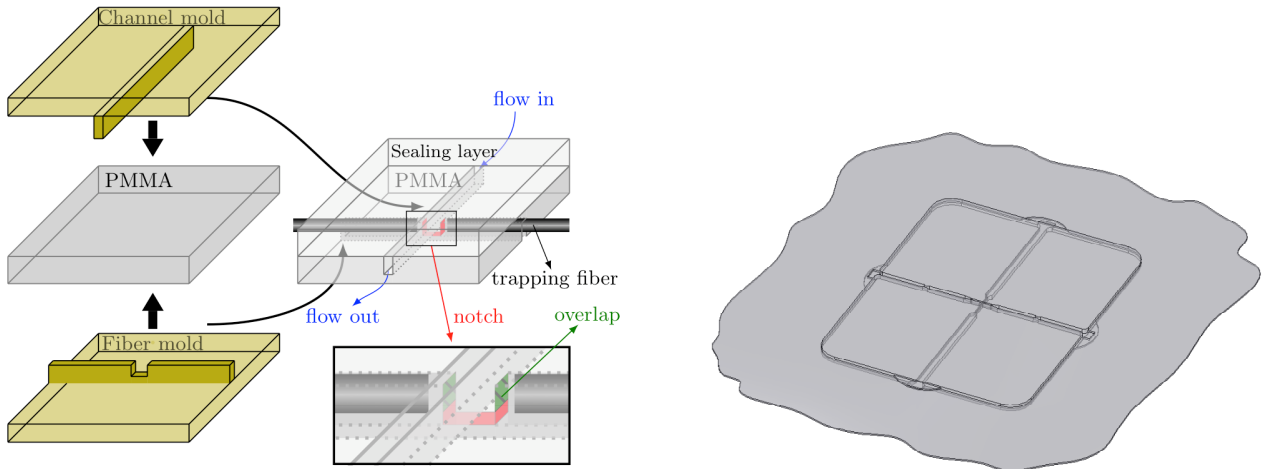

Figure 4: (a) Schematic of the double-sided hot embossing process of a 500µm thick PMMA layer (not on scale). The channel mold and the fiber mold are each pressed in one side of the polymer layer. A drawing of the hot embossed chip is shown on the right, together with the trapping fibers, the flow indication and the sealing layer. (b) Spaceclaim drawing of the final chip after pressing the molds into a 500µm PMMA layer. No air gaps are visible at the maximal overlap (120µm), so no contact between the molds is present.

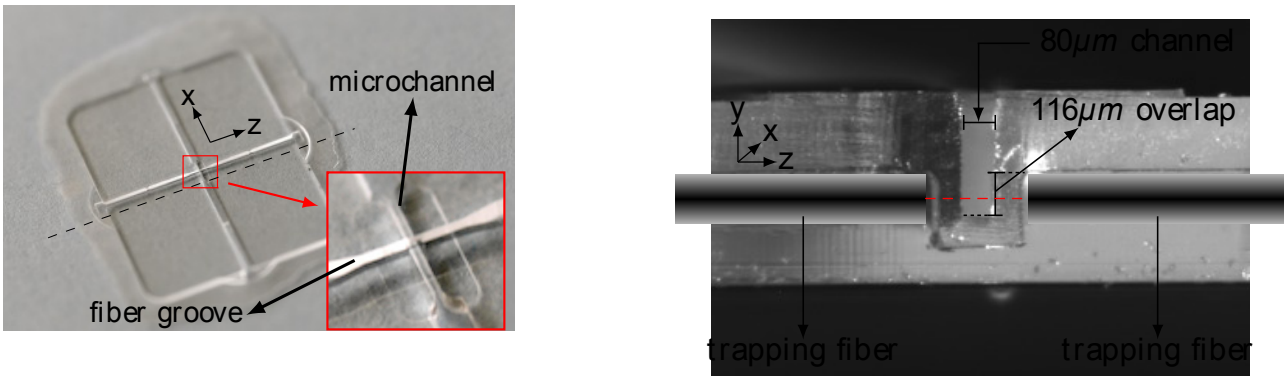

Figure 5: (a) Hot embossed PMMA chip, the chip is milled along the fiber grooves, as indicated by the dashed line; (b) Cross-section of the microchannel at the height of the fiber grooves of a sample from a fully-optimized hot embossing process.

Finally we have sealed the hot embossed microfluidic chip. A top layer with a thickness of 300µm and the same size as the hot embossed layer (20mm by 15mm) is bonded on the latter to seal the microfluidic channel. The bonding is done with a spin coated UV curing adhesive (Loctite 3301, spin coating parameters: 300rpm during 10s and 3500rpm during 10s). The ridges at both sides of the microchannel slow down the capillary force effect and reduce the risk of channel clogging. Nevertheless, care should be taken during this gluing step. We can observe these 500µm ridges at both sides of the microchannel at the top of Figure 5. In a last step, we glued microcapillaries in both ends of the channel to enable a flow of particles. This is done using an UV-curable adhesive. We apply this adhesive at the end of the microfluidic channel after inserting the microcapillary. Due to capillary forces the adhesive will flow inside the channel. With a

strong UV light source the adhesive is cured and the micro-capillary is fixed in the channel. A picture of the final microfluidic chip is shown in Figure 6.

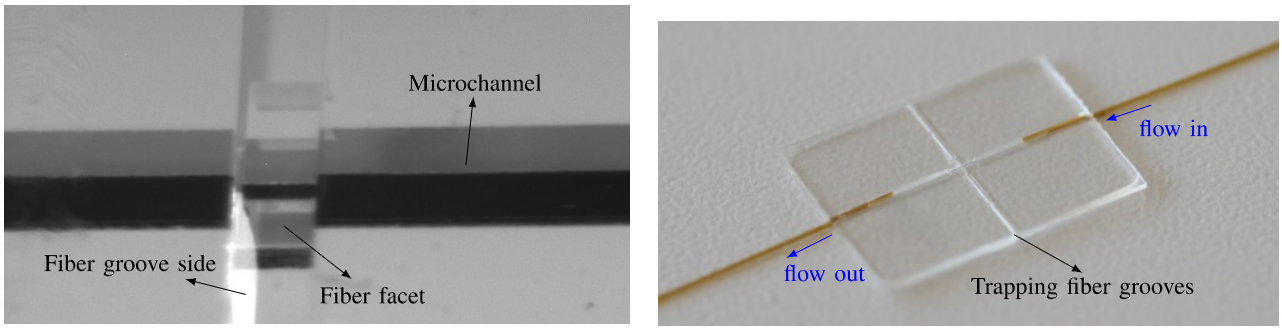

Figure 6: (a) Hot embossed PMMA layer: the fiber grooves are oriented vertically and the microchannel horizontally; (b) Sealed optical trapping chip, as depicted in Figure 4, with microcapillaries at both ends of the channel allowing particles to flow in the microchannel.

4. Proof-of-concept demonstration of optical trapping on-chip

A pigtailed laser (continuous wave, λ=785nm, power at SMF output =280mW) is used to trap particles in the PMMA chip that is clamped on a 3-axis translation stage in the proof-of-concept demonstration setup (Figure 7). The laser light is split by a 50:50 fiber splitter and each output is coupled into a single-mode trapping fiber (MFD = 5µm, NA = 0.13), which is mounted on a 3-axis translation stage. This trapping light is scattered by the trapped bead in the microchannel and is partly captured by an infinity-corrected objective (50X, NA = 0.3). The scattered laser light propagates via a mirror and a dichroic mirror (reflection band 784-786nm) and is finally detected by a position-sensing detector (PSD, Thorlabs PDP90A), that tracks the displacements of the incident light and converts these into voltage signals. The PSD can be rotated and moved in the directions of the optical trap axes (x- and z-direction) to optimize the alignment of the PSD axes with respect to the axes of the optical trap. The PSD uses a variation of the tetra-lateral-type sensor commonly called a "pin cushion" position-sensing device, which moves the anodes to the four corners of the sensors and reshapes the sensor area, to produce a linearity that is comparable with a duo-lateral sensor at a lower cost.

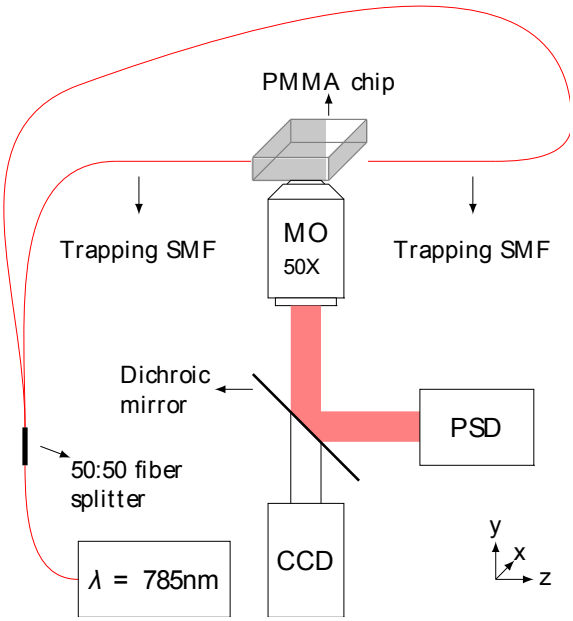

Figure 7: Simplified schematic of the setup (not on scale), showing the trapping fibers inserted in the chip and the detection path, consisting of a microscope objective (MO), a position-sensing detector (PSD) and a CCD camera.

The device is sensitive to wavelengths in the range from 320 to 1100nm, its active area is 9x9mm^2 at the waist of the pincushion and its bandwidth is 15kHz. The photosensitivity at 785nm is approximately 0.5A/W

In our measurement setup we are interested in the frequency content of the bead displacements, explained below, and will use the non-normalized differential signals Δx and Δz for the trap characterization. The dichroic mirror allows the visible light to reach a CCD camera for visual observation of a trapping event. The position-sensing detector is connected to a T-Cube Controller that outputs the x-channel and z-channel voltage signals, respectively representing the axial and transverse bead displacements in the trap, and the sum signal. Each voltage signal is fed into an anti-alias filter to eliminate unwanted high frequency noise. Each filter is shielded to avoid electronic crosstalk between the channels. The filtered voltage signals are subsequently sampled at 20kHz and acquired during 40s using a data acquisition card, controlled by our Labview program. Since very small bead displacements are measured in this proof-of-concept demonstration setup, possible external vibrations and noise sources from the measurement environment have to be eliminated by using for example a damped optical table and by shielding the electronic circuit.

We introduce polystyrene beads (Polysciences, Inc) with a diameter of approximately 6μm (5.941μm±0.123μm), 8μm (8.3μm, relative standard deviation 5 to 10%) and 10μm (10.0μm±0.56μm) in the microchannel. To determine the strength of the harmonic restoring forces and thus the trap strength that can be achieved in the hot embossed chip, we use the power spectrum analysis of the bead displacements to find the trap stiffness [17]. From the frequency content of the bead displacement around the equilibrium position, we can determine the trap stiffness via the corner frequency of the power spectrum. When a bead is trapped between two Gaussian beams it executes a Brownian motion in a harmonic potential well. The resulting forces from these Gaussian beams on the bead are approximately linear in the bead displacements with respect to its equilibrium position, for small bead displacements. The combination of the random Brownian motion and the restoring forces results in a Gaussian distribution of positions, which are tracked by the position-sensing detector. The physics of the Brownian motion in a harmonic potential can be exploited. The power spectrum of the thermal fluctuations is calculated from these time series of voltages. The main idea is that the frequency content of the particle motion is related to the strength of the trap. When the trap stiffness increases, higher frequency components will start dominating the particle movement. The calculated power spectrum is fitted with a Lorentzian spectrum [10].

We record ten time series of 40sec of bead displacements for a bead size with a diameter of 6μm, 8μm and 10μm in a square microcapillary and the optical trapping chip at different trapping powers. Next, the power spectrum of each time series is calculated and fitted with a Lorentzian spectrum in a frequency range from 5Hz to 2000Hz. The average transverse stiffness (κ_x) of the trap is calculated from the corner frequencies fc of the power spectra. These are plotted for the three bead sizes together with the 50% confidence interval error bars in Figure 8 [10].

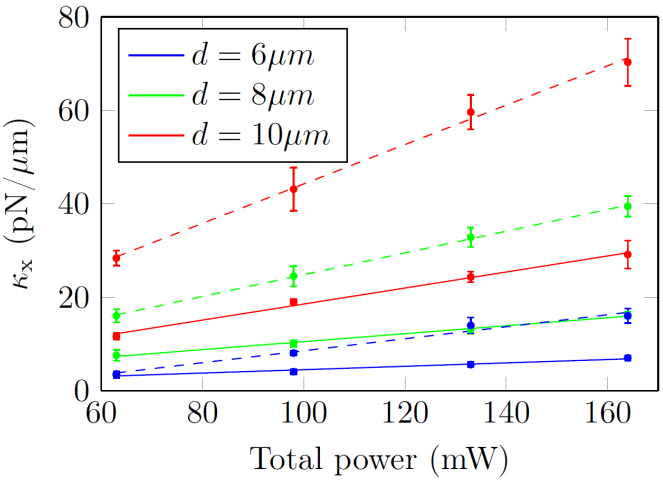

Figure 8: Transverse trap stiffness κ_x as a function of the total trapping power for a 6μm, 8μm and 10μm bead in a square capillary (dashed line) and the optical trapping chip (solid line).

We clearly see a dependency of the trapping stiffness on the trapping power, the bead size and the fiber separation. A higher power leads to a stronger trap and larger beads experience larger optical forces compared to smaller ones. The graph shows a lower trapping stiffness in the chip than in the square capillary which means that the optical trap is weaker in the chip because of the larger fiber separation, as predicted by our model. However, we observe that the measured transverse trapping stiffnesses are larger than the simulated values by an average factor of approximately 3, which could be due to the underestimation of the trapping stiffness in our model or by a systematic error in the measurement setup. A further elaboration on the model could be for example realized by exporting the field that propagated from the fiber exit to the virtual plane in front of the bead from ASAP and use a full-wave method, such as the finite-difference time domain (FDTD) method, to simulate the interaction of this field with the bead. However, this kind of simulations takes several hours. Our model is less accurate but it is a good tool to predict the optical trapping behavior in various situations. Due to an unwanted low frequency drift of the bead we were not able to measure the axial trapping stiffness. Since the axial forces are weak, the expected corner frequency corresponding to these axial stiffnesses is situated below 2Hz and could not be properly fitted in this area. Nevertheless, we were able to demonstrate the trapping capabilities of the hot embossed chip and to characterize the trap strength in the transverse direction for beads with a diameter of 6μm, 8μm and 10μm in a square capillary and in the hot embossed lab-on-chip device.

5. Conclusion

In this paper we presented the miniaturization and integration of optical trapping on-chip. We presented an optical trapping simulation model based on wave-optics and ray-tracing and used this model as a tool to design a microfluidic chip for dual fiber optical trapping. We developed a low-cost, robust PMMA chip design on 100μm thin pieces of PMMA. We presented the design, simulation, fabrication process and proof-of-concept demonstration of this chip, fabricated through ultraprecision diamond tooling and double-sided hot embossing. We showed the trapping capability of the hot embossed chip by trapping polystyrene beads with a diameter of 6μm, 8μm and 10μm.

Acknowledgments

The authors would like to thank Dries Rosseel and Kurt Rochlitz for their technical support in the fabrication of the molds, the hot embossing of the optical trapping chip and the Multisensor Coordinate Measurement Machine measurements on the molds. J. Van Erps acknowledges the financial support of the FWO Vlaanderen under a postdoctoral Research Fellowship. This work was supported in part by FWO (G008413N), IWT, the MP1205 COST Action, BELSPO IAP Photonics@be, the Methusalem and Hercules foundations, Flanders Make, and the OZR of the Vrije Universiteit Brussel.

References

[1] U. Neugebauer, S. Dochow, C. Krafft, T. Bocklitz, J. H. Clement, and J. Popp, "Diagnostics of tumor cells by combination of Raman spectroscopy and microfluidics," Proc. SPIE 8087, 1–11 (2011).

[2] D. De Coster, D. Loterie, H. Ottevaere, M. Vervaeke, J. Van Erps, J. Missinne, and H. Thienpont, "Free-form optics enhanced confocal Raman spectroscopy for optofluidic lab-on-chips," IEEE J. Sel. Topics Quantum Electron. 21, 1–8 (2015).

[3] R.Wilson, S. A. Bowden, J. Parnell, and J. M. Cooper, "Signal enhancement of surface enhanced Raman scattering and surface enhanced resonance Raman scattering using in situ colloidal synthesis in microfluidics," Anal. Chem. 82, 2119–2123 (2010).

[4] A. Ashkin, "Acceleration and trapping of particles by radiation pressure," Phys. Rev. Lett. 24, 156–159 (1970).

[5] K. C. Neuman and S. Block, "Optical trapping," Rev. Sci. Instrum. 75, 2787–2809 (2004).

[6] K. Svoboda and S. M. Block, "Biological applications of optical forces," Annu. Rev. Biophys. Biomol. Struct. 23, 247–285 (1994).

[7] K. C. Neuman and S. Block, "Optical trapping," Rev. Sci. Instrum. 75, 2787–2809 (2004).

[8] F. Merenda, J. Rohner, J.-M. Fournier, and R.-P. Salathé, "Miniaturized high-NA focusing-mirror multiple optical tweezers," Opt. Express 15, 6075–6086 (2007).

[9] E. Sidick, S. Collins, and A. Knoesen, "Trapping forces in a multiple-beam fiberoptic trap," Appl Opt. 36, 6423–6433 (1997).

[10] D. De Coster, H. Ottevaere, M. Vervaeke, J. Van Erps, M. Callewaert, P. Wuytens, S. Simpson, S. Hanna, W. De Malsche, and H. Thienpont, "Mass-manufacturable polymer microfluidic device for dual fiber optical trapping," Opt. Express 23, 30991–31009 (2015).

[11] E. Aspnes, T. D. Milster, and K. Visscher, "Optical force model based on sequential ray tracing," Applied optics 48, 1642–1650 (2009).

[12] L. Ferrara, E. Baldini, P. Minzioni, F. Bragheri, C. Liberale, E. D. Fabrizio, and I. Cristiani, "Experimental study of the optical forces exerted by a Gaussian beam within the Rayleigh range," J. Opt. 13, 075712 (2011).

[13] I. Sraj, A. C. Szatmary, D. W. M. Marr, and C. D. Eggleton, "Dynamic ray tracing for modeling optical cell manipulation," Opt. Express 18, 16702–16714 (2010).

[14] T. Cižmár, O. Brzobohatý, K. Dholakia, and P. Zemánek, "The holographic optical micro-manipulation system based on counter-propagating beams," Laser Phys. Lett. 8, 50–56 (2011).
[15] E. Sidick, S. Collins, and A. Knoesen, "Trapping forces in a multiple-beam fiberoptic trap," Appl Opt. 36, 6423–6433 (1997).
[16] "Refractive index database," http://refractiveindex.info/. (Accessed in September 2013).
[17] K. Berg-Sørensen and H. Flyvbjerg, "Power spectrum analysis for optical tweezers," Rev. Sci. Instrum. 75, 594–612 (2004).